Clogauite, $PbBi_4Te_4S_3$, a new member of the aleksite series

Nigel J. Cook[1,*], Cristiana L. Ciobanu[1], Jie Yao[1], Christopher J. Stanley[2], Wenyuan Liu[3], Ashley Slattery[4], Benjamin Wade[4]

[1] *School of Chemical Engineering, The University of Adelaide, Adelaide, SA 5005, Australia*

[2] *Department of Earth Sciences, The Natural History Museum, Cromwell Road, London SW7 5BD, United Kingdom*

[3] *College of Zijin Mining, Fuzhou University, Fuzhou 350108, China*

[4] *Adelaide Microscopy, The University of Adelaide, Adelaide, SA 5005, Australia*

Abstract

Clogauite, ideally $PbBi_4Te_4S_3$ is the new n=1 member of the aleksite series, $Pb_nBi_4Te_4S_{n+2}$, where n is the homologue number. Clogauite is named from the type locality, the Clogau gold mine, Dolgellau Gold belt, Gwynedd, North Wales, U.K. The mineral and name have been approved by the IMA Commission on New Minerals and Mineral Nomenclature (proposal 2023-062). The aleksite series is an accretional homologous series in which each member is derived from the same 5-atom tetradymite archetype. Clogauite crystallizes in the trigonal crystal system (space group: *P*-3*m*1, # 164). Three distinct polytypes of clogauite are recognized, corresponding to identical chemistry but different layer sequences, expressed as (57), (5559) and (557.559), respectively, in reference to the number of atoms in individual layer sequences. These are clogauite-*12H*, a = 4.277(4) Å, c =

* Corresponding author: nigel.cook@adelaide.edu.au

Mineralogical Society

This is a 'preproof' accepted article for Mineralogical Magazine. This version may be subject to change during the production process.
DOI: 10.1180/mgm.2024.46

23.46(14) Å, V = 371.598 Å^3, Z = 1; clogauite-*24H*, a = 4.278(4) Å, c = 46.88(31) Å, V = 743.053 Å^3, Z = 2; and clogauite-*36H*, a = 4.278(4) Å, c = 70.36(32) Å, V = 1115.283 Å^3, Z = 3. Clogauite is opaque, with a pale grey colour in reflected light. Reflectance is higher than tetradymite or galena. Bireflectance and anisotropy are strong. Structural data was determined from measurement of atomic-scale HAADF STEM imaging showing the internal arrangement of component atoms and characteristic selected area electron diffraction patterns for each polytype. The structures were then further constrained from *ab initio* total energy calculations and structure relaxation using density functional theory (DFT) using the measured parameters as input data. The relaxed crystal structure for each polytype was modelled to generate crystallographic information file (cif) data files. STEM and electron diffraction simulations based on the crystallographic information data obtained from the DFT calculations show an excellent match to the empirical measurements.

Keywords: clogauite; new mineral; aleksite series; bismuth-lead chalcogenides; Clogau gold mine.

Introduction

Lead-Bi-chalcogenides of the aleksite series, with the general chemical formula $Pb_nBi_4Te_4S_{n+2}$ (Cook *et al.*, 2007a, 2019; Yao *et al.*, 2023) occur as accessory phases in several gold-bearing ore deposits. The aleksite series is a prime example of mixed layer compounds built by accretional homology principles. Series members are structurally derived from the same tetradymite archetype and are related to the tetradymite group of bismuth chalcogenides (Cook *et al.*, 2007b; Ciobanu *et al.* 2009, 2021; Yao *et al.*, 2024). The three named minerals in the series prior to the acceptance of clogauite are aleksite ($PbBi_2Te_2S_2$; Lipovetskiy *et al.*, 1978), saddlebackite ($Pb_2Bi_2Te_2S_3$; Clarke, 1997) and hitachiite ($Pb_5Bi_2Te_2S_6$; Kuribayashi *et al.*, 2019) (Fig. 1A).

Clogauite, $PbBi_4Te_4S_3$, is the fourth member of the series to be named and corresponds to "Phase C" of Lipovetskiy *et al.* (1976). It also corresponds to Phase D synthesized experimentally at 500 °C by Liu and Chang, (1994). An unnamed phase with the same composition was previously reported by Bevins and Stanley (1990), Clarke (1997) and Cook *et al.* (2007a), while Bonev and Neykov

https://doi.org/10.1180/mgm.2024.46 Published online by Cambridge University Press

(1990) reported 'lead tetradymite', an analogous phase to clogauite of similar composition, with Pb-content between the compositions of tetradymite and aleksite. In all cases, clogauite co-exists with, or is observed in the same samples as aleksite.

Clogauite has been approved by the IMA Commission on New Minerals and Mineral Nomenclature (proposal 2023-062). Preliminary optical and compositional characterization of $PbBi_4Te_4S_3$ was given by Cook *et al.* (2007a). Cook *et al.* (2019) presented results of a nanoscale study using high angle annular dark field scanning transmission electron microscope (HAADF STEM) imaging and STEM energy-dispersive X-ray spectrometry (EDS) analysis that confirmed the existence of three distinct polytypes: 57, 557.559 and 5559, after the arrangement of layer stacks. Each polytype has a total number of atoms in the layer stacks, 12, 24 and 36, which is divisible by three. Therefore, the trigonal space group $P\bar{3}m1$ was considered instead of $R\bar{3}m$, in agreement with the symmetry considerations of Imamov and Semiletov (1971). The notation *H* (hexagonal) of Frangis *et al.* (1990) was adopted for all polytypes.

Clogauite is named for the Clogau gold mine, Dolgellau Gold belt, Gwynedd, North Wales, U.K. (52° 45' 42" North, 3° 58' 5" West), where type material was sampled and studied. The proposed abbreviation symbol for clogauite (Warr, 2021) is Clg. The holotype is represented by specimen E.1309 from the collection of the Natural History Museum (U.K.), corresponding to National Museum of Wales NMW specimen number NMW 90.37 G.M1 and M2a and b (Bevins and Stanley, 1990).

Occurrence

Clogauite type material is a specimen representative of high-grade gold veins in the Clogau deposit (Bevins and Stanley, 1990). Background information on the locality is given by Dominy and Platten (2012). The specimen contains lamellar intergrowths of clogauite, aleksite, galena, tellurobismuthite, and minor chalcopyrite, with traces of native gold. A complete description of the sample, including reflected light images and electron probe microanalytical data, is provided in Cook *et al.* (2007a) and

https://doi.org/10.1180/mgm.2024.46 Published online by Cambridge University Press

Cook *et al.* (2019). Back-scatter electron (BSE) imaging at high-magnification emphasizes that many of the coarser lamellae in the specimen feature fine-scale, partially disordered intergrowths of multiple Pb-Bi-chalcogenides of both the aleksite series and tetradymite group (tellurobismuthite and tetradymite). Clogauite is defined from analysis of a single lamella, roughly 160 μm across, that appeared compositionally homogeneous on BSE images and electron microprobe element maps.

Optical and physical properties

Clogauite occurs as fine lamellae, exceptionally up to as much as 160 μm in width. Colour (macroscopic), streak, lustre, hardness, cleavage, fracture and parting: could not be directly observed due to the size of the mineral. Streak can, however, be inferred from the black colour of the fine powder used for an X-ray diffraction (XRD) investigation by one of us (C.J.S.) early in the study. Lustre, hardness, and other physical properties can be expected to closely resemble those of tetradymite (e.g., metallic lustre). Calculated densities are 7.3724, 7.3738, and 7.3691 g/cm^3 for clogauite-12*H*, -24*H*, and -36*H*, respectively, based on the empirical formula. Density could not be measured because there is insufficient material. Clogauite is non-magnetic and twinning is not observed.

Clogauite is opaque. Its colour in reflected light is pale grey, with reflectance higher than tetradymite and galena (Fig. 1a). Bireflectance and pleochroism are both distinct, anisotropy is strong. Internal reflections are not observed. Full reflectance data for the phase now named as clogauite were provided by Cook *et al.* (2007a). Reflectance values (%R_0, $R_{e'}$, $^{im}R_0$ and $^{im}R_{e'}$) at λ = 470 nm are: 52.7, 52.5, 38.8, and 36.8; 53.7, 51.6, 39.4, and 37.3 at 546 nm; 53.8, 51.7, 39.4, and 37.4 at 589 nm; and 53.75, 51.6, 39.2, and 37.2 at 650 nm.

Chemical composition

Quantitative mineral compositional data and EPMA measurement conditions were given by Cook *et al.* (2019). The mean composition based on measurement of 57 points is 12.56 wt.% Pb, 49.45 Bi, 30.62 Te, 6.42 S, 0.12 Se (Total 99.18). The empirical formula is

https://doi.org/10.1180/mgm.2024.46 Published online by Cambridge University Press

$Pb_{0.98}Bi_{3.84}Te_{3.89}(S_{3.26}S_{0.02})_{3.28}$ based on a total of 12 atoms. This composition defines a small field on a plot of Pb/(Pb+Bi) vs. (Te+Se)/(Te+Se+S) (Fig. 1b, c). The simplified formula corresponds to the ideal formula $PbBi_4Te_4S_3$, which requires Pb 12.58 wt.%, Bi 50.76 wt.%, Te 30.99 wt.% and S 5.84 wt.%, total 100 wt%. A confirmation of chemical homogeneity was afforded by EPMA element maps (Cook *et al.*, 2019). The combination of spot analysis and element mapping served as a basis to identify suitable areas of the lamella to extract by focused ion beam (FIB)-scanning electron microscope methods for subsequent transmission electron microscope study.

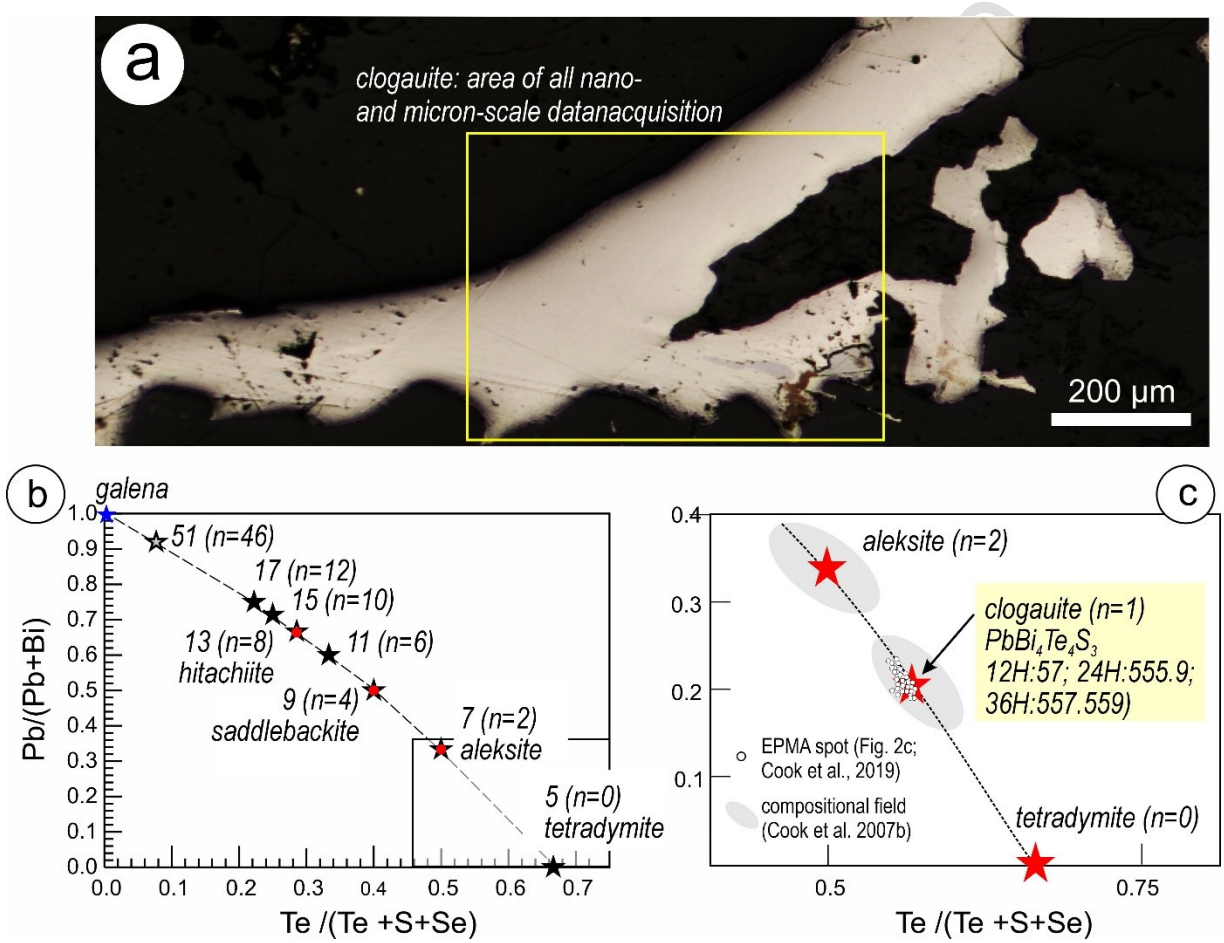

Figure 1. (a) Reflected light image of clogauite lamella on which all analytical data was collected. **(b)** Composition of previously named minerals in the aleksite series in terms of the ratios Pb/(Pb+Bi) vs. Te/(Te+S+Se). **(c)** EPMA data for clogauite plotted on a reduced portion of the same diagram.

Crystal structure

Work on synthetic $PbBi_4Te_4S_3$ gave cell dimensions where a = 4.24 Å and c = 23.12 Å (Liu and Chang, 1994). Unpublished X-ray diffraction data on $PbBi_4Te_4S_3$ in Clogau material by one of us

https://doi.org/10.1180/mgm.2024.46 Published online by Cambridge University Press

(C.J.S.) in the early 1990s (reported in Cook *et al.*, 2007a), gave cell dimensions of a = 4.25 Å and c = 69.71 Å. The discrepancy in c dimensions was later explained (Cook *et al.*, 2019) through observation of distinct layer arrangements (polytypes) yet the same composition. The synthetic $PbBi_4Te_4S_3$ of Liu and Chang corresponds to clogauite-12*H*, and the aforementioned earlier X-ray diffraction to clogauite-36*H*.

The co-existence of all three polytypes in the same holotype was confirmed by HAADF STEM imaging and STEM EDS mapping of the structures to show the internal arrangement of component atoms (Cook *et al.*, 2019). All HAADF STEM imaging and energy-dispersive X-ray spectrometry (EDS)-STEM mapping was performed using an ultra-high resolution, probe-corrected, FEI Titan Themis S/TEM housed at Adelaide Microscopy, The University of Adelaide, and operated at 200 kV. Further details of instrumentation were provided in Cook *et al.* (2019). TIA and Velox software were used for image acquisition, including drift-corrected frame integration package (DCFI), and EDS data acquisition and processing. Various filters (Radial Wiener, High-pass, Average and Gaussian blur) were used to eliminate noise. Indexing of diffraction patterns was conducted with WinWulff© (JCrystalSoft) Crystal structure models were generated in CrystalMaker® and image simulations using STEM for xHREM™ software.

A foil extracted from chemically homogenous lamella in Figure 1a shows the three distinct polytypes are intergrown with one another as distinct stacking sequences along the c axis, but with intervals of regular repeats of at least ~150 nm (Fig. 2a, b). In the example shown in Figure 2, the polytype with the simplest (5.7) stack is the most common and occurs as repeats across distances as large as 350 nm. The polytype with the longest (557.559) stack is second most common, as repeats across ~100-200 nm. The third polytype, sequence 555.9, is the scarcest of the three. An interval of 41 stacks of the sequence 5.7 (simplest polytype) is shown on the images in Figure 2c.

https://doi.org/10.1180/mgm.2024.46 Published online by Cambridge University Press

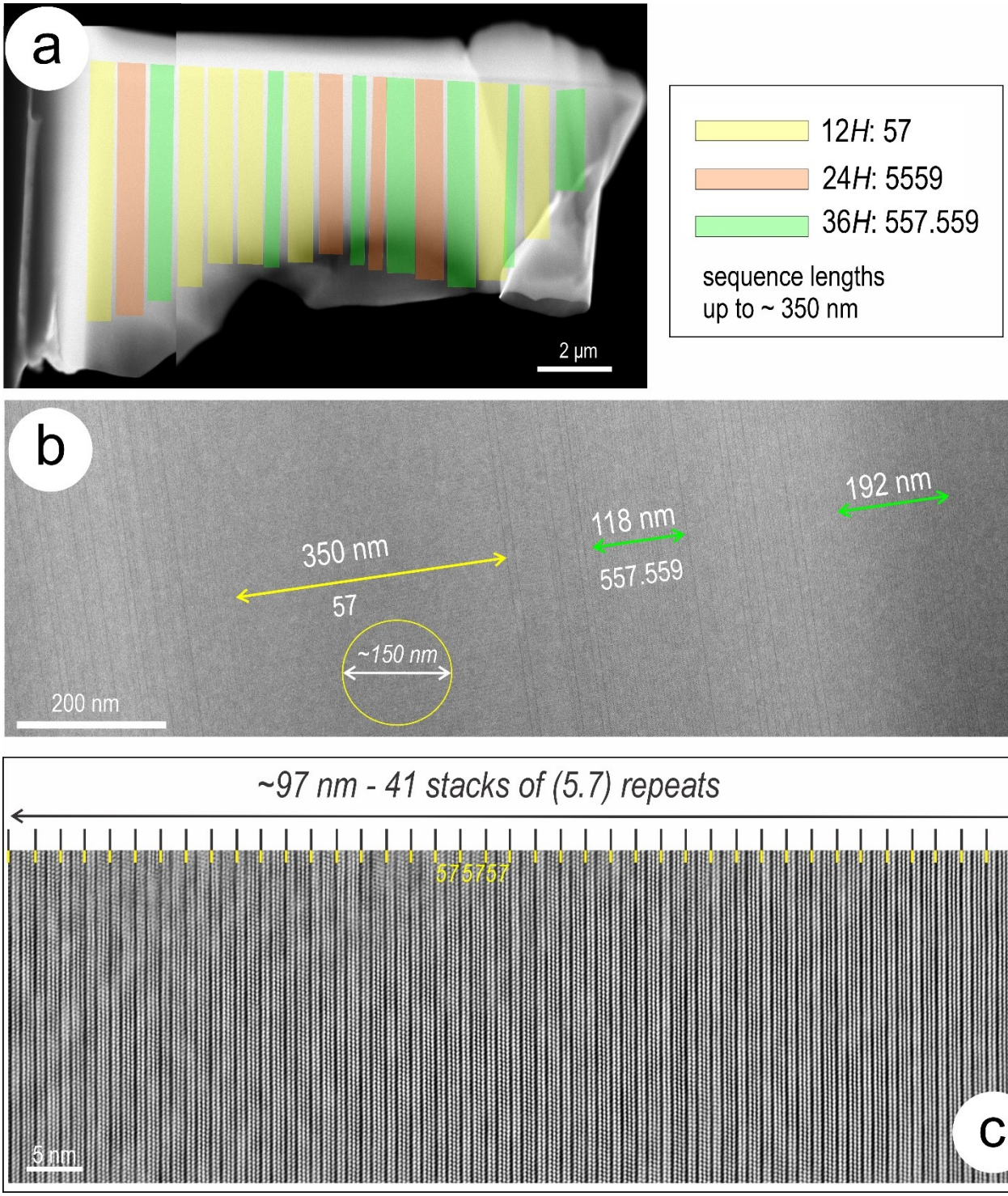

Figure 2. (**a**) Low-magnification view of entire thinned foil showing the distribution of the three polytypes as marked. (**b**) HAADF STEM images of clogauite showing a longer ~350 nm-long interval of polytype (57) (yellow arrows) and shorter, ~100–200 nm nm-long intervals (green arrows) of the (557.559) polytype interspersed with more disordered stacking sequences. Yellow circle shows the approximate area (diameter ~150 nm), for selected area electron diffractions acquisition. Note intervals marked for the 36*H* polytype indicating 17 (118 nm) and 27 (192 nm) unit cells. (**c**) Sequence of 41 consecutive stacks of the (57) polytype. Images (a) and (b) are modified from Cook *et al.* (2019).

https://doi.org/10.1180/mgm.2024.46 Published online by Cambridge University Press

The three polytypes, shown as high-resolution HAADF STEM images with specimen tilted on $[2\bar{1}\bar{1}0]$ zone axis (Fig. 3), are interpreted in terms of the following arrangements:

i. (57) Regular combinations of 5-atom (Te-Bi-S-Bi-Te) and 7-atom (Te–Bi–S–Pb–S–Bi–Te) layers, 12*H* (Fig. 3a);

ii. (5559) Regular combinations of three 5-atom and one 9-atom (Te–Bi–S–Pb–S–Pb–S–Bi–Te) layers, 24*H* (Fig. 3b);

iii. (557.559) Ordered combinations of two groups of layer stacks: two 5-atom and one 7-atom layers (557) followed by two 5-atom and one 9-atom layers (559), 36*H* (Fig. 3c).

Van der Waals bonds (often called gaps in the earlier literature) occur between Te atoms at the edge of neighboring units (dark lines on HAADF STEM images), so that the individual layers (5, 7, 9) are well separated from one another. The *c* parameter corresponds to the length of a single stack sequence and is directly measurable from images, i.e., *c*~24 Å, ~47 Å, and ~70 Å for 12*H*, 24*H*, and 36*H*, respectively (Fig. 3).

https://doi.org/10.1180/mgm.2024.46 Published online by Cambridge University Press

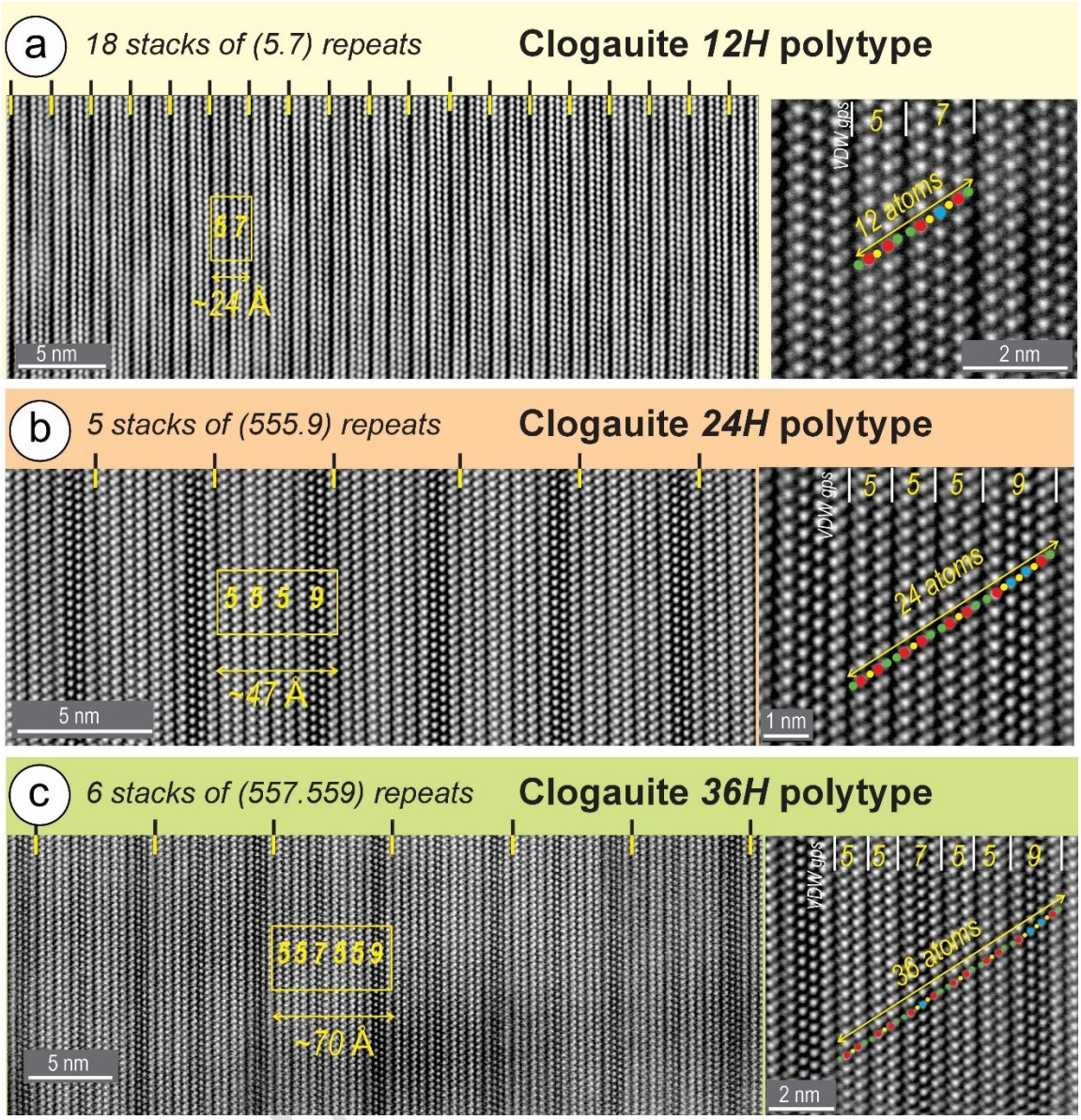

Figure 3. HAADF STEM images with specimen tilted on the $[2\bar{1}\bar{1}0]$ zone axis showing longer stacks representing the three polytypes of clogauite as labelled. A single unit cell of each repeat sequences, i.e., (57), (5559), and (557.559), is marked in a rectangle on each panel (**a**, **b**, **c**), and enlarged on the right to emphasize the contained atoms.

In HAADF STEM imaging mode, the signal intensity (I) is dependent upon the atomic number (Z) of the chemical element, i.e., $I \sim Z^2$. On the images in Figure 3, the brighter dots represent Bi (Z=83) and Pb (Z=82) atoms, whereas the less bright dots on the margins of each module correspond to Te atoms (Z=52). Light sulphur atoms (Z=16) are not depicted on these images. The 5-, 7- and 9-atom layers show 2, 3, and 4 bright dots, respectively, accounting for Bi and Pb atoms. The number of lighter atoms (Te and S) are 3, 4 and 5. HAADF signal profiles across sequences comprising the

https://doi.org/10.1180/mgm.2024.46 Published online by Cambridge University Press

three types of layers show a decrease in signal for Pb relative to Bi across 7- and 9-atom layers, whereas Te is marked by shoulders on the signal for Bi, and S is not depicted (Fig. 4). The position of Pb in the middle of 7- and 9-atom layers indicated by the profiles in Fig. 4b is also shown on high-resolution EDS STEM element maps (Fig. 4c). Positions of the chalcogen atoms, Te and S, relative to Bi and Pb are concordant with the atom sequences marked on Figure 3a-c.

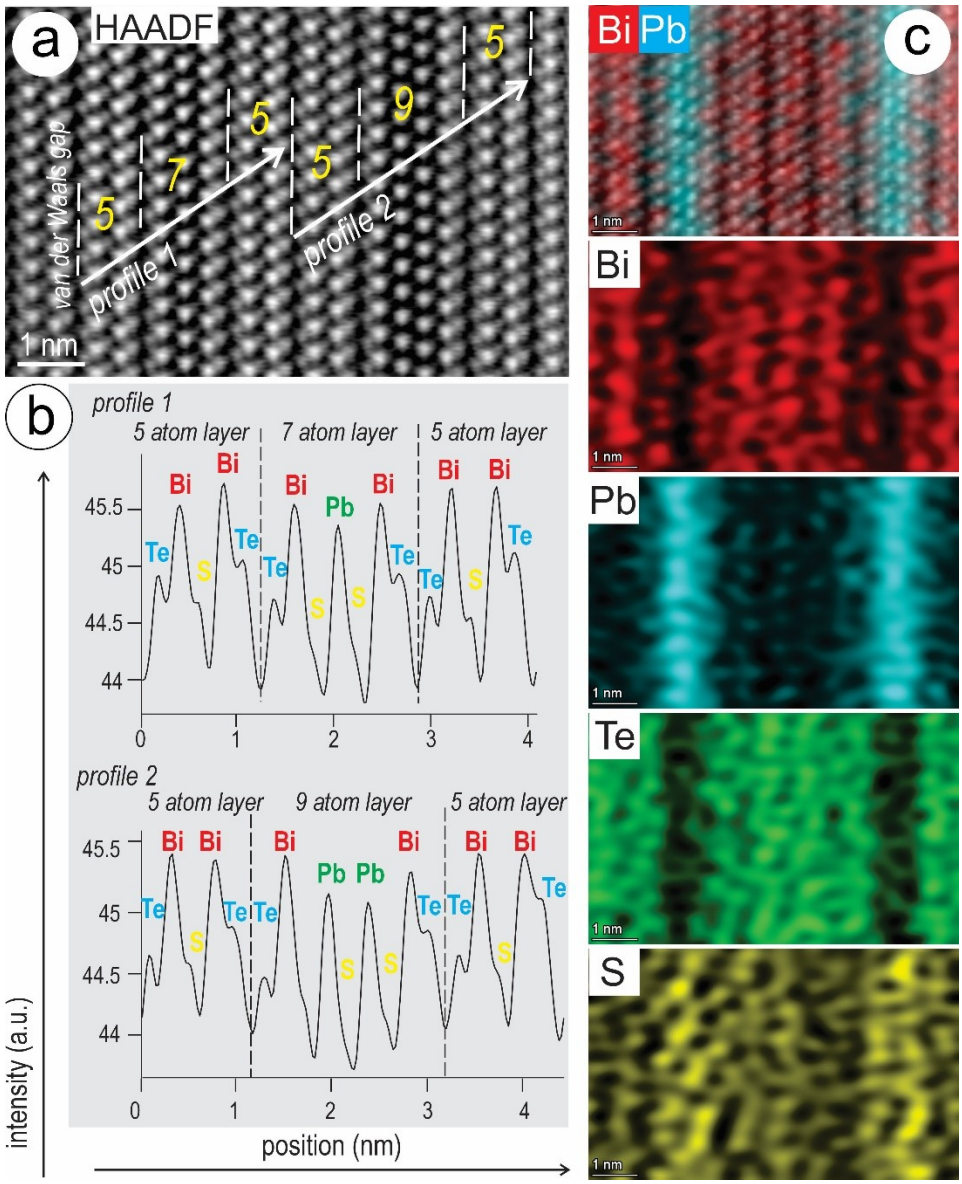

Figure 4. (**a**) HAADF STEM image showing two profiles, each comprising three layer stacks as labelled. (**b**) HAADF signal intensity (black line) across the two profiles depicting the sequences and their contained atoms, i.e., double, triple, and quadruple peaks for the five-, seven-, and nine-atom units. Note that Bi atoms are picked out by highest intensity, followed by Pb. Sulphur atoms have the lowest intensity signals. (**c**) HAADF STEM image and STEM EDS element maps, as marked, showing arrangement of atoms across a (5559) stack.

https://doi.org/10.1180/mgm.2024.46 Published online by Cambridge University Press

Selected area electron diffraction (SAED) patterns on $[2\bar{1}\bar{1}0]$ zone axis for each polytype show common features such as modulation along c^*, with strongest reflections defining the interlayer interval d* of comparable length (d=1/d* in the range 1.9 and 1.98 Å for each polytype; see table 4 in Cook *et al.* (2019). Measurements of d_a are in the range 3.7–3.5 Å, giving parameters for a between 4.27 Å and 4.5 Å when using the formula: $a=d_a/\cos 30^o$. The smaller value is close to a=4.24 Å obtained for the synthetic analogue of clogauite (Liu and Chang, 1994). We note that $(01\bar{1}0)$ and $(02\bar{2}0)$ reflections are present on SAEDs (e.g., Fig. 5a) which is indicative of space group $P\bar{3}m1$.

Clogauite poytypes can, however, be differentiated by (a) number of satellite reflections and their intensity along the d* interval defining 12, 24 and 36 equal divisions corresponding to total number of layers (N) for each polytype, i.e., 12*H*, 24*H* and 36*H*, and (b) the number of divisions in the central part of d* (between the pair of satellites of strongest intensity by the middle of d*), i.e., 2, 4 and 6 for polytypes with sequences 57, 555.9, and 557.559, respectively (Fig. 5).

https://doi.org/10.1180/mgm.2024.46 Published online by Cambridge University Press

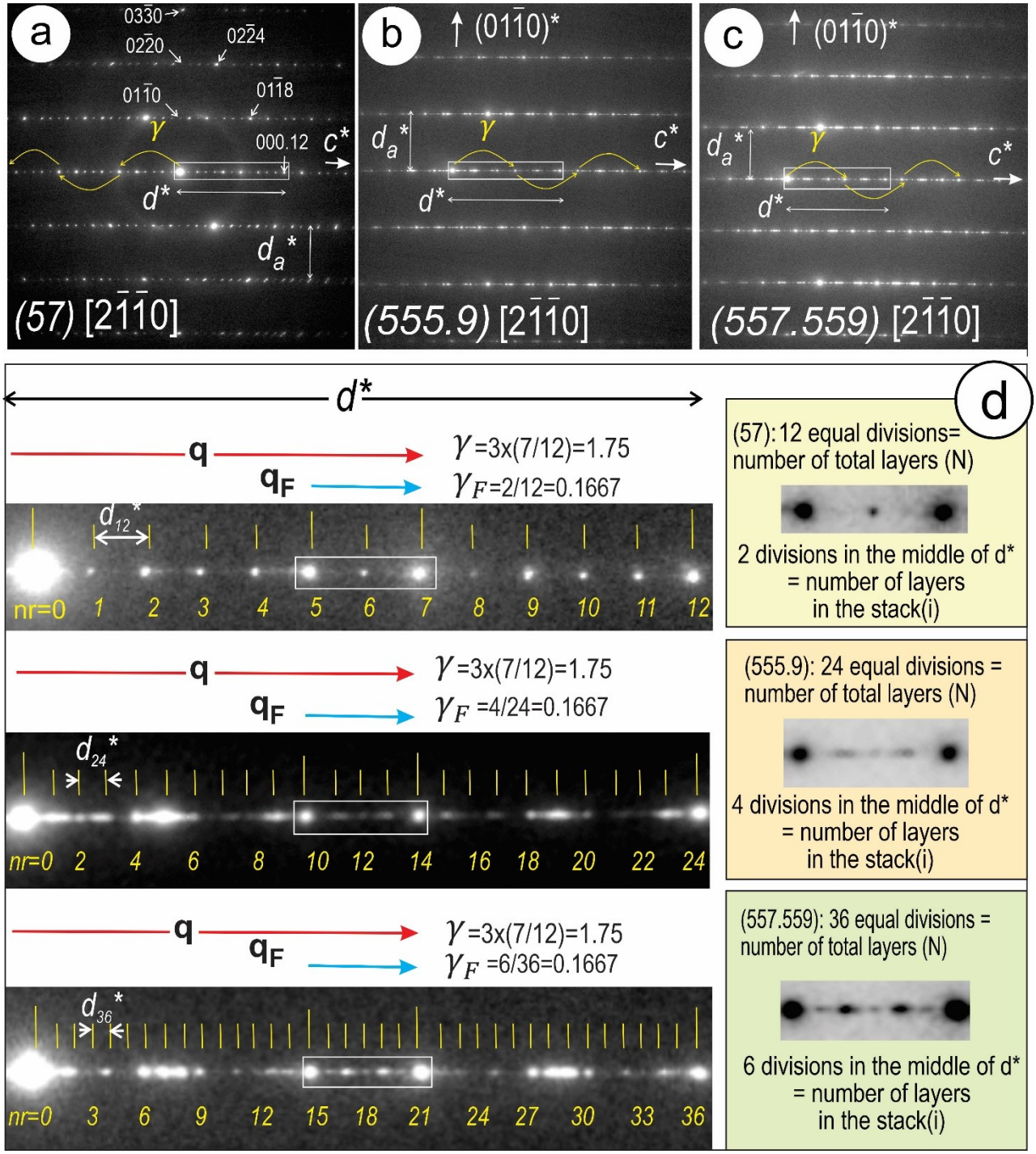

Figure 5. (a-c) Selected area electron diffraction (SAED) for each polytype with specimen tilted on [2$\bar{1}\bar{1}$0] zone axis. The d*~2Å interval marked on the SAED patterns represents the $d^*_{subcell}$ for each polytype. Arrows indicate the satellite reflections depicted by γ modulation along c^*. (**d**) Schematic showing that the three polytypes are N superstructures of the $d^*_{subcell}$ (explanations to the right). The equal divisions defined by the satellite reflections (yellow lines) and their intensity variation across d* (crop from each SAED pattern) are well defined. The number of divisions within the central part of d* (between the brightest two reflections) corresponding to the modulation vector q_F are visible on the SAED patterns. The distances between two satellite reflections is d_N (example d_{12}) and represents the *c* parameter for *H* phases.

https://doi.org/10.1180/mgm.2024.46 Published online by Cambridge University Press

The measured crystal structures identified in Cook *et al.* (2019) were further constrained from *ab initio* total energy calculations and structure relaxation based on density functional theory (DFT). Calculations were performed with the Vienna *ab initio* simulation package (VASP; (Kresse and Furthmüller, 1996), using the projector augmented wave (PAW) method. A plane wave basis set with energy cut-off of 600 eV was employed for all calculations. The electronic exchange and correlation energy were estimated by the generalized gradient approximation (GGA) with revised parameters of Perdew *et al.* (2008). The calculations incorporated the van der Waals interactions between atoms of the same type (Te-Te) using the method of Grimme *et al.* (2010), which adds a small dispersion energy correction to the total energy in the system. The Brillouin zone (BZ) was sampled at Γ-centred dense k-point grids based on the Monkhorst-Pack scheme. Further experimental details are given in Tables 1 and 2.

Volumes from the input file were considered as V_i. Unit-cell parameters *(a, c)* were subsequently scaled in the range 95 to 101% to obtain a series of volume values. Total energy calculations and structural optimization for the atomic positions and the two cell parameters were carried out with energy tolerance $<10^{-7}$ eV between two ionic steps and force less than 0.02 eV/Å per atom. After volume relaxation, a static calculation is performed to obtain the total energy. Figure 6 is a plot of V/atom *vs*. E_0/atom for the three structures.

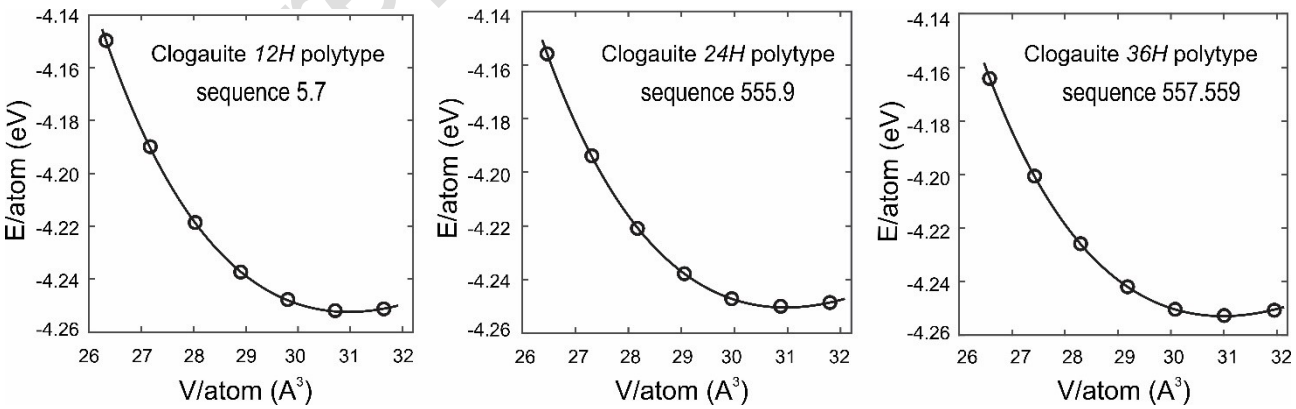

Figure 6. Plot of V/atom vs. E_0/atom for the three structures.

The relaxed crystal structures for the three polytypes of clogauite were modelled and assessed using CrystalMaker software and Findsym was used to generate the three crystallographic

https://doi.org/10.1180/mgm.2024.46 Published online by Cambridge University Press

information file (cif) data files. Electron diffractions and STEM image simulation were performed using STEM for xHREM^{TM} software for structure visualization.

Clogauite crystallizes in the Trigonal crystal system (space group *P*-3*m*1, # 164). Modelling results show that values for *a* are the same for the three polytypes. Cell dimensions and volumes are as follows: Clogauite-*12H* (57): $a = 4.277(4)$ Å, $c = 23.46(14)$ Å, $V = 371.598$ Å^3, $Z = 1$; clogauite-*24H (5559),* $a = 4.278(4)$ Å, $c = 46.88(31)$ Å, $V = 743.053$ Å^3, $Z = 2$; and clogauite-*36H, (557.559),* $a = 4.278(4)$ Å, $c = 70.36(32)$ Å, $V = 1115.283$ Å^3, $Z = 3$.

Tables 3a-c list atom coordinates and Wyckoff positions for the three polytypes. Respective bond distances are given in Table 4a-c. Figures 7 and 8 show the structures of the three polytypes and the bonds within the asymmetric unit cell as constructed using CrystalMaker. STEM and electron diffraction simulations (Fig. 9) based on the crystallographic information data obtained from the DFT calculations show an excellent match to analytical data (Figs. 3, 5) and as given by Cook *et al.* (2019). Two equivalent zone axes were chosen, $[2\bar{1}\bar{1}0]$ and $[11\bar{2}0]$, for analytical and simulations, respectively.

https://doi.org/10.1180/mgm.2024.46 Published online by Cambridge University Press

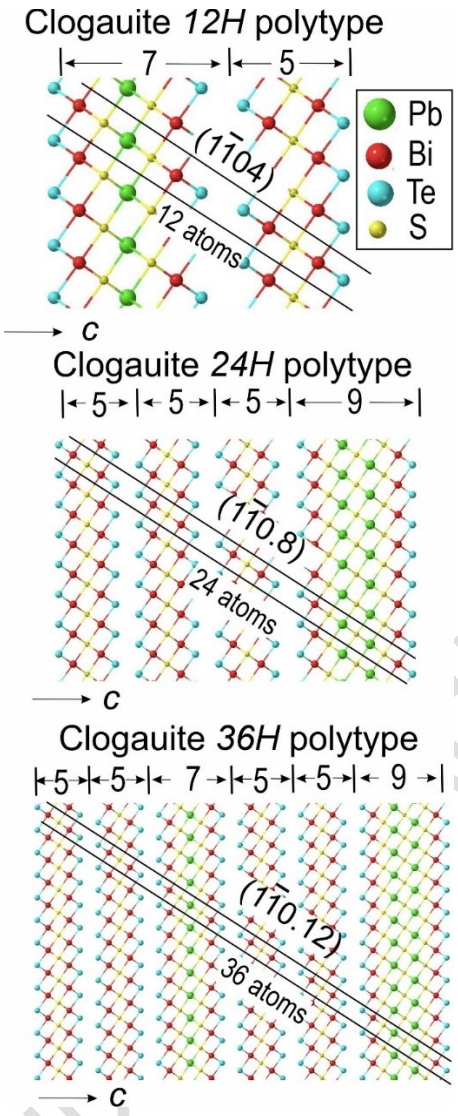

Figure 7. Crystal models plotted on [11$\bar{2}$0] zone axis as ball and stick representations showing the structures of the three clogauite polytypes as labelled.

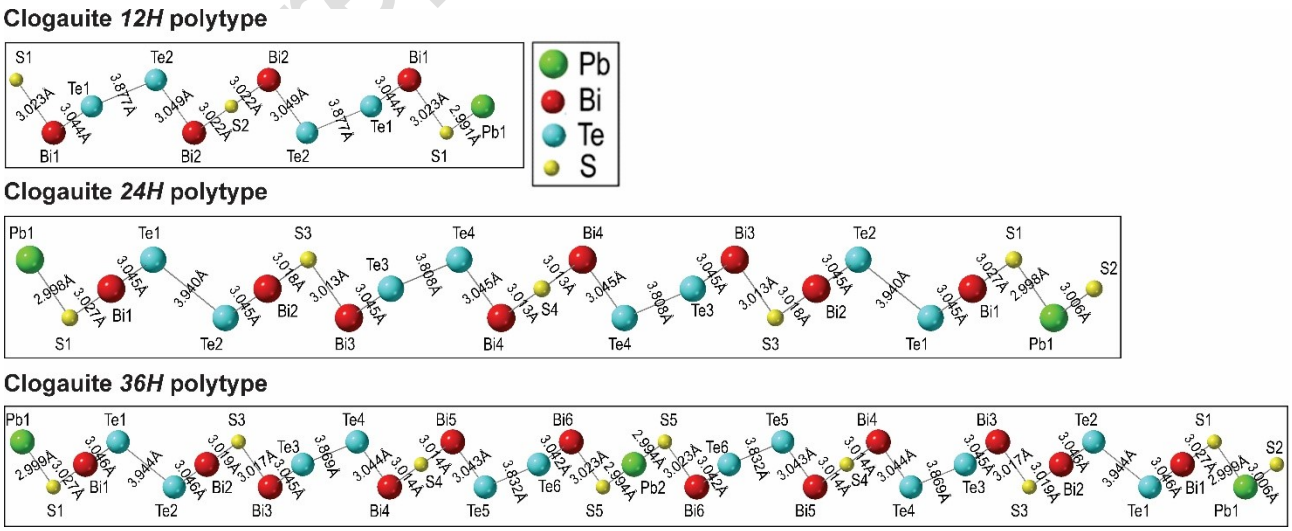

Figure 8. Bond types and lengths for the relaxed structures of the three clogauite polytypes plotted on [11$\bar{2}$0] zone axis. Red–Bi, blue–Te, yellow–sulfur, green–Pb.

https://doi.org/10.1180/mgm.2024.46 Published online by Cambridge University Press

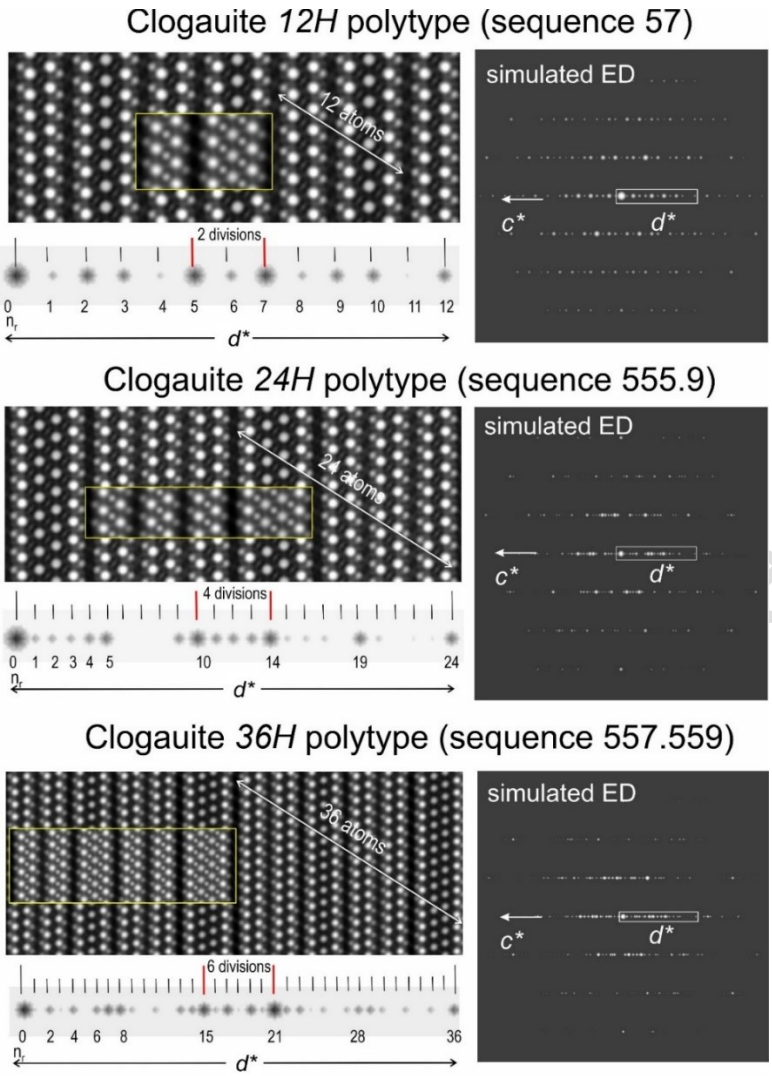

Figure 9. STEM simulations (left) and electron diffraction (right) on $[11\bar{2}0]$ zone axis using the crystallographic information data obtained by DFT calculations. This zone axis is equivalent to $[2\bar{1}\bar{1}0]$ used in Cook *et al.* (2019). Insets on the three images (yellow boxes) show the same structures but using Se instead of S to highlight the presence and location of the chalcogen atoms. The d* interval beneath each STEM simulation shows the number of reflections (n_r). The number of divisions within the two brighter reflections by the middle of d* (2, 4, and 6) corresponds to the number of building modules in each polytype.

Discussion

Modularity across what has been informally referred to as the aleksite series after the first named mineral, aleksite, is depicted from the building modules formed by incremental addition of nPbS layers and leading to a homologous series with the formula: $Pb_nBi_4Te_4S_{n+2}$, where n represents homologue number (Cook *et al.*, 2007a). Compositions where n=2k, where k is an integer value, correspond to single-layer structures, e.g., aleksite (n=2), saddlebackite (n=4), and hitachiite (n=10),

https://doi.org/10.1180/mgm.2024.46 Published online by Cambridge University Press

whereas those with n = 2k + 1 integer values are formed by combinations of modules as in clogauite (n=1).

The generic formula for the series was revised as $Pb_{(n-1)}Bi_2X_{n+2}$ (n = homologue number, X=chalcogen) (Moëlo *et al.*, 2008). Cook *et al.* (2007a) postulated the existence of a hierarchical series of Pb-Bi-tellurosulphides that can be expanded from the archetypal 5-atom tetradymite unit to larger 7-, 9-, 11-atom units, whereas Moëlo *et al.* (2008) considered the tetradymite (Bi_2Te_2S) archetype as a link to layered sulfosalts. The same approach was taken by Kuribayashi *et al.* (2019) when describing hitachiite as n=6 according to the formula of Moëlo *et al.* (2008).

Relationships between the aleksite and tetradymite series of mixed layer compounds

Yao *et al.* (2023) used DFT to obtain structural data for the aleksite series, including two polytypes each of aleksite (aleksite-21*R* and -42*R*) and saddlebackite (saddlebackite-9*H* and -18*H*), hitachiite, and the n=6, n=8, and n=12 homologues not yet observed in natural specimens ($Pb_6Bi_4Te_4S_8$, $Pb_8Bi_4Te_4S_{10}$ and $Pb_{12}Bi_4Te_4S_{14}$). This study followed the mixed-layer compound concept for series of Bi-chalcogenides whereby modulation vectors along c* defined from diffractions patterns underpin chemical variation in a predictable and quantifiable manner (Amelinckx *et al.*, 1989; Frangis *et al.*, 1990; Ciobanu *et al.*, 2009).

Prior to such TEM studies, a model for the derivation of rhombohedral crystal structures from the system Bi-Te (and comparable Bi-Se and Sb-Te systems) was proposed from basic principles of chemistry and crystallography (Imamov and Semiletov, 1971, and references therein). This model postulated (i) two fixed-width modules with stacks: Te-Bi-Te-Bi-Te (notation 5) and Bi-Bi (notation 2), which are combined in different proportions to facilitate chemical variation within the series; and (ii) calculation of lattice parameters using those known for Bi_2Te_3 and Bi. The 5- and 2-stack model was later formalised as $nBi_2.mBi_2Te_3$, where n and m are integers, for homologous series of layered tetradymite-like compounds (Shelimova *et al.*, 2000).

https://doi.org/10.1180/mgm.2024.46 Published online by Cambridge University Press

Criticism of this model came from Frangis *et al.* (1990) that showed an alternative derivation of modules from Bi_2Te_3, as the initial basic structure, to account for chemical variation of compounds in the range $Bi_{2+\delta}Te_3$ ($\delta<1$), e.g., addition of Te-Bi instead of Bi-Bi to the same Te-Bi-Te-Bi-Te stack. Therefore, there are two module types of 7-atom layers, which are structurally identical with one another yet have different Bi and Te configurations, symmetrical and asymmetrical, and different compositions (Bi_3Te_4 and Bi_4Te_3, respectively). Frangis *et al.* (1990) defined a modulation vector ($\mathbf{q_F}$-notation from Ciobanu *et al.*, 2009) that relates the 7- and 9-atom building modules in the derived structures to basic structures (BS), e.g., 5 as BS for 7, 7 as BS for 9, and so on, via the fractional shift method of Van Landyut *et al.* (1970).

Ciobanu *et al.* (2009) used the mixed layer compounds approach to interpret the modularity of natural phases from the tetradymite series in the range Bi_2Te_3-Bi_8Te_3 studied by HR-TEM. The authors provided a homology formula, $S'(Bi_{2k}X_3)\cdot L'[Bi_{2(k+1)}X_3]$, where X = chalcogen, and S′ and L′ are the number of short and long modules with asymmetric Bi and Te arrangements, respectively. This is different to the homology using modules of fixed width (Shelimova *et al.*, 2000). The model also differs that of Frangis *et al.* (1990), which uses symmetrical modules, yet shares the same accretional building principle, i.e., modules of incremental rather than fixed widths.

The revised model of Ciobanu *et al.* (2009) was validated by electron diffraction patterns that showed all phases are N-fold superstructures (N = number of layers in the stacking sequence) of a rhombohedral subcell with $c/3 = d_1 \sim 0.2$ nm, positioning of the two brightest reflections about the middle of d_1^*, and a monotonic decrease of two modulations with increasing Bi content. The $\mathbf{q_F}$ modulation of Frangis et al. (1990) was adapted to incorporate the homology for S′, L′ modules underpinned by k as: $\mathbf{q_F} = \gamma_F c_{sub}^*$; $\mathbf{q_F} = (i/N)d_1^* = id_N^*$, $i = S' + L'$, relating changes in module size and number to displacements in a basic substructure. The displacements are quantifiable by fractional shifts between reflections in the derived and basic structures. A second modulation, $\mathbf{q} = \gamma c_{sub}^*$ ($\mathbf{q} \sim$ homoatomic interval; $\gamma = 1.8$–1.64 for the Bi_2Te_3-Bi_8Te_3 analytical range; $c_{sub} \sim 3d_1$), based on the displacive modulation between chalcogen and Bi atoms was adapted from Lind and Lidin (2003).

https://doi.org/10.1180/mgm.2024.46 Published online by Cambridge University Press

DFT and STEM simulations study of the tetradymite series in the same range of compositions (Bi_2Te_3-Bi_8Te_3) has confirmed the mixed-layer compound model (Yao *et al.*, 2024).

Ciobanu *et al.* (2009) also stipulated that compounds with symmetrical modules discussed by Frangis *et al.* (1990), obtained by addition of n(M-X; M=metal; X=chalcogen, Te, Se, S) layers form a chalcogen-rich isoseries with the tetradymite series postulated to exhibit comparable modulations vectors along c^*. HAADF STEM imaging has shown the differences between the asymmetrical (Ciobanu *et al.*, 2021; Cook *et al.*, 2021) and symmetrical modules (Cook *et al.*, 2019). The identity of the 7-, 9-, and 11-symmetrical layer stacks is shown for clogauite in the new set of images in the present contribution (Figs. 3 and 4).

Concordant with the concept of mixed layer compounds, the SAED patterns for clogauite display two brightest reflections about the middle of d* and are described by the following two modulations:

(1) $\mathbf{q} = \gamma \bullet c^*_{sub}$ ($\mathbf{q}$ ~ homoatomic interval; calculated $\gamma = 1.75$ for all polytypes, c_{sub} ~3d); and

(2) $\mathbf{q_F} = \gamma_F \bullet c^*_{sub}$; $\mathbf{q_F} = (i/N) \bullet d^* = i \bullet d_N^*$, i = S + L, S, L = number of longer and shorter modules with symmetrical M (M=Pb, Bi) and Te arrangements, γ_F =0.1667 for all polytypes (Fig. 5).

Based on the relaxed structures, the d interval is 1.955, 1.953, and 1.954 Å for the 12*H*, 24*H,* and 36*H* polytypes, respectively.

DFT calculations combined with a STEM simulation study of structures in the aleksite series for homologues with even number in the compositional range between n=0 and n=12 (Yao *et al.*, 2023) shows *a* and *c* values within 1.5% of experimental data and both *a* and the interlayer distance d_{sub} (the equivalent notation used here is d) decreasing as the PbS content increases. The study also showed simulated electron diffraction patterns that have two brightest reflections at the centre of d^*_{sub}, and are described by monotonic decrease of the two displacive modulations as described above, with γ_F=0.2–0.059 and γ = 1.8 to 1.588 for the compositional range. Importantly, the linear relationship between γ and d_{sub} allows prediction of any theoretical phases in the series. The study of (Yao *et al.*, 2023) demonstrated the likely upper compositional limit of the aleksite series at as n=398

https://doi.org/10.1180/mgm.2024.46 Published online by Cambridge University Press

($Pb_{398}Bi_4Te_4S_{400}$) but also the strong likelihood that additional members will be discovered and that at least some may exist as multiple polytypes.

Relationships between γ and d_{sub} for the two Bi-chalcogenide series discussed here show that isostructural phases share the same γ values, but with d values slightly lower for aleksite relative to corresponding tetradymite compounds (Yao *et al.*, 2023, 2024), e.g. clogauite and tsumoite (BiTe) both have γ=1.75 but their d values are ~1.953-1.955 Å and 1.996 Å, respectively.

The results outlined above validate the crystal-structural formula for aleksite series as: $S(M_pX_{p+1}).L(M_{p+1}X_{p+2})$, where M=Pb,Bi, and X=Te,S, $p \geq 2$, and S and L are the number of short and long modules with symmetric M-X arrangement, respectively (Cook *et al.*, 2019; Yao *et al.*, 2023).

The alternative model of homology using modules of fixed size nPbTe.$m$$Bi_2Te_3$ introduced by Shelimova *et al.* (2004) and adopted by Kuribayashi *et al.* (2019) does not depict the displacive modularity introduced by the layer arrangements, even though it may be conceptually useful to depict chemical variation within the aleksite series. For example, clogauite-12*H* would have m=2 and n=1, so three building modules instead of two (5- and 7-atom layers). The displacive modulation $\mathbf{q_F}$ along c^* shows there are two and not three modules, i.e., there are two divisions between the two brightest reflections by the middle of the d* interval. This mixed-layer compounds model allows prediction of the series that is checked by the correspondence between the number of layers (N), building modules (incremental blocks with uneven number of atoms), characteristics of electron diffraction patterns, and indeed the *ab initio* study of Yao *et al.* (2023).

Summary

Bismuth-Pb-chalcogenides of the informally named aleksite series, $Pb_nBi_4Te_4S_{n+2}$ (Cook *et al.*, 2007a) are a modular series derived from tetradymite (Bi_2Te_2S). Cook *et al.* (2019) gave an overview of named, unnamed, and predicted species in the aleksite series. The same paper introduced a homology for the series, where the phase now named as clogauite is the n=1 homologue member,

aleksite is n=2, saddlebackite is n=4, and hitachiite, n=10. Multiple polytypes are a feature of the series, including two for aleksite (21*R*, 42*R*) and three for saddlebackite (9*H*, 18*H*, 54*H*), all supported by published data, as well as the approximate unit cell dimensions of predicted and inadequately characterized series members.

The three clogauite structures discussed here can be regarded as polytypes because they have the same chemistry but differ in terms of the stacking sequences, concordant with Hatert *et al.* (2023). Each chemically distinct species within the aleksite series is a polysome or homologue, whereas phases with the same chemistry but different stacking sequences, like clogauite, not affecting their chemistry – these are polytypes. The modularity of the three polytypes is recognised on their electron diffractions, atomic-scale images, and STEM simulations. Best fits for the cell dimensions are obtained from the DFT calculations. The $\mathbf{q_F}$* modulation depicts the number of building modules by the divisions between the two brightest reflections in the middle of d interval.

Supplementary materials

Crystallographic information file (cif) data files for clogauite-12*H*, -24*H*, and -36*H* are available at….. ….

Acknowledgements: The authors acknowledge Microscopy Australia for instrument access. Comments from two anonymous reviewers assisted us to improve clarity and expression.

Competing interests: The authors declare none.

References

Amelinckx S., Van Tendeloo G., Van Dyck D. and Van Landuyt J. (1989) The study of modulated structures, mixed layer polytypes and 1-D quasi-crystals by means of electron microscopy and electron diffraction. *Phase Transitions*, **16**, 3–40.

Bevins R.E. and Stanley C.J. (1990) Aleksite, a lead bismuth sulfotelluride: A second world occurrence from the Dolgellau Gold belt, Gwynedd, Wales. *Journal of the Russell Society*, **3**, 67–69.

https://doi.org/10.1180/mgm.2024.46 Published online by Cambridge University Press

Bonev I.K. and Neykov H.N. (1990) Minerals of silver, bismuth and tellurium in Ardino polymetallic deposit. *Bulgarian Academy of Science, Geokhimiya, Mineralogiya i Petrologiya*, **26**, 3-19.

Ciobanu C.L., Pring A., Cook N.J., Self P., Jefferson D., Dima G.I. and Melnikov V. (2009) Chemical-structural modularity in the tetradymite group: A HRTEM study. *American Mineralogist*, **94**, 517–534.

Ciobanu C.L., Slattery A.D., Cook N.J., Wade B.P. and Ehrig K. (2021) Bi_8Te_3, the 11-atom layer member of the tetradymite homologous series. *Minerals*, **11**, 980.

Clarke R.M. (1997) Saddlebackite, $Pb_2Bi_2Te_2S_3$, a new mineral species from the Boddington gold deposit, Western Australia. *Australian Journal of Mineralogy*, **3**, 119–124.

Cook N.J., Ciobanu C.L., Stanley C.J., Paar W. and Sundblad K. (2007a) Compositional data for Bi-Pb tellurosulfides. *The Canadian Mineralogist*, **45**, 417–435.

Cook N.J., Ciobanu C.L., Wagner T. and Stanley C.J. (2007b) Minerals of the system Bi-Te-Se-S related to the tetradymite archetype: Review of classification and compositional variation. *The Canadian Mineralogist*, **45**, 665–708.

Cook N.J., Ciobanu C.L., Liu W.Y., Slattery A., Wade B.P., Mills S. and Stanley C.J. (2019) Polytypism and polysomatism in mixed-layer chalcogenides: characterization of $PbBi_4Te_4S_3$ and inferences for ordered phases in the aleksite series. *Minerals*, **9**, 628.

Cook N.J., Ciobanu C.L., Slattery A.D., Wade B.P. and Ehrig K. (2021) The Mixed-Layer Structures of Ikunolite, Laitakarite, Joséite-B and Joséite-A. *Minerals*, **11**, 920.

Dominy S. and Platten I.M. (2012) Gold mineralisation and ore controls at the Clogau mine, Dolgellau, North Wales, United Kingdom. *Applied Earth Sciences, IMM Transactions*, **B121**, 12–28.

Frangis N., Kuypers S., Manolikas C., Van Tendeloo G., Van Landuyt J. and Amelinckx S. (1990) Continuous series of one-dimensional structures in compounds based on M_2X_3 (M = Sb, Bi, X = Se, Te). *Journal of Solid State Chemistry*, **84**, 314–334.

Grimme S., Antony J., Ehrlich S. and Krieg H. (2010) A consistent and accurate ab initio parametrization of density functional dispersion correction (DFT-D) for the 94 Elements H-Pu. *Journal of Chemical Physics*, **132**, 154104.

Hatert F., Mills S., Pasero M., Miyawaki R. and Bosi F. (2023) CNMNC guidelines for the nomenclature of polymorphs and polysomes. *Mineralogical Magazine*, **87**, 225-232.

https://doi.org/10.1180/mgm.2024.46 Published online by Cambridge University Press

Imamov P.M. and Semiletov S.A. (1971) The crystal structure of the phases in the system Bi-Se, Bi-Te, and Sb-Te. *Soviet Physics, Crystallography*, **15**, 845–850.

Kresse G. and Furthmüller J. (1996) Efficient iterative schemes for ab initio total-energy calculations using a plane-wave basis set. *Physical Review B*, **54**, 11169–11186.

Kuribayashi T., Nagase T., Nozaki T., Ishibashi J., Shimada K., Shimizu M. and Momma K. (2019) Hitachiite, $Pb_5Bi_2Te_2S_6$, a new mineral from the Hitachi mine, Ibaraki Prefecture, Japan. *Mineralogical Magazine*, **83**, 733-739.

Lipovetskiy A.G., Borodaev Y.S. and Zav'yalov Y.N. (1979) Aleksite, $PbBi_2Te_2S_2$, a new Mineral. *International Geology Review*, **21**, 1223–1228.

Liu H. and Chang L.L.Y. (1994) Lead and bismuth chalcogenide systems. *American Mineralogist*, **79**, 1159–1166.

Moëlo Y., Makovicky E., Mozgova N.N., Jambor J.L., Cook N., Pring A., Paar W., Nickel E.H., Graeser S., Karup-Møller S., Balic-Žunic T., Mumme W.G., Vurro F., Topa D., Bindi L., Bente K. and Shimizu M. (2008) Sulfosalt systematics: A review. Report of the sulfosalt sub-committee of the IMA Commission on Ore Mineralogy. *European Journal of Mineralogy,* **20**, 7–62.

Perdew J.P., Ruzsinszky A., Csonka G.I., Vydrov O.A., Scuseria G.E., Constantin L.A., Zhou X. and Burke K. (2008) Restoring the Density-Gradient Expansion for Exchange in Solids and Surfaces. *Physical Review Letters*, **100**, 136406.

Shelimova L.E., Karpinskii O.G., Svechnikova T.E., Avilov E.S., Kretova M.A. and Zemskovet V.S. (2004) Synthesis and structure of layered compounds in the PbTe–Bi_2Te_3 and PbTe–Sb_2Te_3 systems. *Inorganic Materials,* **40**, 1264–1270.

Van Landuyt J., De Ridder R., Gevers R. and Amelinckx S. (1970) Diffraction effects due to shear structures: A new method for determining the shear vector. *Materials Research Bulletin*, **5**, 353–362.

Warr, L. (2021) IMA–CNMNC approved mineral symbols. *Mineralogical Magazine*, **85**, 291-320.

Yao J., Ciobanu C.L., Cook N.J. and Ehrig K. (2023) *Ab initio* crystal structures and phase stabilities for the aleksite series, $Pb_nBi_4Te_4S_{n+2}$. *Acta Crystallographica B*, **79**, 482-494.

Yao J., Ciobanu C.L., Cook N.J., Ehrig K., Dima G. and Steinle-Neumann G. (2024) *Ab initio* calculations and crystal structure simulations for mixed layer compounds from the tetradymite series. *American Mineralogist*, in press; https://doi.org/10.2138/am-2023-9018.

https://doi.org/10.1180/mgm.2024.46 Published online by Cambridge University Press

Table 1. Number of atoms and chemical formula units applied in each simulation box and KPOINTS grids for the three clogauite structures.

	57	5559	557559
Number of atoms	12	24	36
Formula units	1	2	3
KPOINTS mesh	20x20x4	11x11x1	16x16x1

Table 2. Equation of state parameters fitted from the energy volume relation for the three $PbBi_4Te_4S_3$ structures. V_0 represents the equilibrium volume for each simulation cell, K_0 and K_0' are the bulk modulus and its derivative. The elastic properties are compared with experimental and previously published calculations. See also Figure 8.

	E_0/atom (eV)	V_0/atom (Å^3)	K_0 (GPa)	K_0'
57 (12*H*)	-4.25	30.97	29	7.4
5559 (24*H*)	-4.25	30.96	29	7.7
557.559 (36*H*)	-4.25	30.98	28	7.8

Table 3a. Atom coordinates and Wyckoff positions for clogauite-12*H*.

	x/*a*	*y*/*b*	*z*/*c*	*Occupancy*	*Wyckoff position*
Bi1	0.33333	0.66667	0.85374	1.00	2d
Bi2	0.33333	0.66667	0.57425	1.00	2d
Pb1	0.00000	0.00000	0.00000	1.00	1a
Te1	0.00000	0.00000	0.77787	1.00	2c
Te2	0.33333	0.66667	0.34953	1.00	2d
S1	0.33333	0.66667	0.07194	1.00	2d
S2	0.00000	0.00000	0.50000	1.00	1b

https://doi.org/10.1180/mgm.2024.46 Published online by Cambridge University Press

Table 3b. Atom coordinates and Wyckoff positions for clogauite-24*H*.

	x/a	*y/b*	*z/c*	*Occupancy*	*Wyckoff position*
Bi1	0.00000	0.00000	0.88987	1.00	2c
Bi2	0.00000	0.00000	0.25160	1.00	2c
Bi3	0.33333	0.66667	0.67459	1.00	2d
Bi4	0.33333	0.66667	0.53680	1.00	2d
Pb1	0.33333	0.66667	0.03654	1.00	2d
Te1	0.33333	0.66667	0.14813	1.00	2d
Te2	0.33333	0.66667	0.78640	1.00	2d
Te3	0.00000	0.00000	0.36338	1.00	2c
Te4	0.33333	0.66667	0.42520	1.00	2d
S1	0.33333	0.66667	-0.07280	1.00	2d
S2	0.00000	0.00000	0.00000	1.00	1a
S3	0.33333	0.66667	0.28860	1.00	2d
S4	0.00000	0.00000	0.50000	1.00	1b

Table 3c. Atom coordinates and Wyckoff positions for clogauite-36*H*.

	x/a	*y/b*	*z/c*	*Occupancy*	*Wyckoff position*
Bi1	0.00000	0.00000	-0.07340	1.00	2c
Bi2	0.00000	0.00000	-0.16776	1.00	2c
Bi3	0.33333	0.66667	0.78296	1.00	2d
Bi4	0.33333	0.66667	0.69006	1.00	2d
Bi5	0.33333	0.66667	0.35903	1.00	2d
Bi6	0.33333	0.66667	0.45117	1.00	2d
Pb1	0.33333	0.66667	0.02435	1.00	2d
Pb2	0.00000	0.00000	0.50000	1.00	1b
Te1	0.33333	0.66667	0.09873	1.00	2d
Te2	0.33333	0.66667	0.85757	1.00	2d
Te3	0.00000	0.00000	0.24234	1.00	2c
Te4	0.33333	0.66667	0.28466	1.00	2d
Te5	0.33333	0.66667	0.61571	1.00	2d
Te6	0.00000	0.00000	0.42593	1.00	2c
S1	0.33333	0.66667	-0.04853	1.00	2d
S2	0.00000	0.00000	0.00000	1.00	1a
S3	0.33333	0.66667	0.19243	1.00	2d
S4	0.00000	0.00000	0.33448	1.00	2c
S5	0.33333	0.66667	0.52405	1.00	2d

https://doi.org/10.1180/mgm.2024.46 Published online by Cambridge University Press

Table 4a. Bond distances (Å) for clogauite-12*H*.

Bi1	S1	3.023
Bi1	Te1	3.044
Bi2	S2	3.022
Bi2	Te2	3.049
Pb1	S1	2.991
Te1	Te2	3.877

Table 4b. Bond distances (Å) for clogauite-24*H*.

Bi1	S1	3.027
Bi1	Te1	3.045
Bi2	S3	3.018
Bi2	Te2	3.045
Bi3	S3	3.013
Bi3	Te3	3.045
Bi4	S4	3.013
Bi4	Te4	3.045
Pb1	S1	2.991
Te1	Te2	3.940
Pb1	S2	3.006
Te3	Te4	3.808

Table 4c. Bond distances (Å) for clogauite-36*H*.

Bi1	S1	3.027
Bi1	Te1	3.046
Bi2	S3	3.019
Bi2	Te2	3.046
Bi3	S3	3.017
Bi3	Te3	3.045
Bi4	S4	3.014
Bi4	Te4	3.044
Bi5	S4	3.014
Bi5	Te5	3.043
Bi6	S5	3.023
Bi6	Te6	3.042
Pb1	S1	2.991
Te1	Te2	3.944
Pb1	S2	2.999
Te3	Te4	3.869
Pb2	S5	2.994
Te5	Te6	3.832

https://doi.org/10.1180/mgm.2024.46 Published online by Cambridge University Press